International Journal of Control and Automation
Vol. 9, No. 10 (2016), pp.315-326
http//dx.doi.org/10.14257/ijca.2016.9.10.29

# Control Strategy of Voltage Source Converter Based High Voltage Direct Current System Based On Active Disturbance Rejection Control

Hu Xiangjuan[1]

[1]*Department of Information Engineering, Shaoyang Univerity, Hunan Prov., Shaoyang, 422000*
*huxiangjuan@126.com*

***Abstract***

*Voltage source converter based high voltage direct current (VSC-HVDC) system technique has been widely applied in the field of power transmission, system control strategy of VSC-HVDC system based on active disturbance rejection control (ADRC) is proposed aiming at low stability precision and weak anti-jamming capability issues of traditional PI control. The structure diagram of system control is designed according to mathematical model of VSC-HVDC system built, of which ADRC strategy is adopted in sending system and receiving system. The external loop of sending system adopts Fal function control and inner loop adopts PI control; the external loop of receiving system adopts DC voltage control and inner loop adopts current and reactive power control. At last, simulation experiment is conducted on controller designed through Matlab/Simulink, experimental results show that ADRC based controller, which has a better control performance, reaches stable state before 0.2~0.3 second compared with traditional controller.*

***Keywords****: VSC-HVDC; ADRC; PID control; Pulse width modulation (PWM); Non-linear feedback*

## 1. Introduction

With a growing threat of power shortages and environmental pollution issues, the using scales of renewable energy like wind energy source and solar energy have been expanded, it's not economical to use network service with traditional DC transmission technology due to its inherent dispersibility, small scale and long distance from load center features; local power generation device with stiff price is adopted for some offshore drilling platforms and isolated islands where are shortage of energy load, neither economic nor environmental; in addition, electrical network capacity is required to be expanded with an rapid increase of urban power load, however, given urban population expansion and reasonable urban planning, on the one hand, it's required to use numbered line corridor to deliver more power, on the other hand, it's required that a large of power distribution to shift to ground. That requires a new DC transmission technology to handle above-mentioned issues. However, VSC-HVDC based on voltage source converter (VSC) and pulse-width modulation (PWM) of turn-off device is a solution to this problem [1]. Viewing from technical feature and running condition of practical engineering, it's appropriately applied in the field of renewable energy grid, interconnection of distributed generation, power supply of islets, city power supply, network interconnection of asynchronous communication *etc*. Therefore, VSC-HVDC will play a big role in renovation and capacity expansion of urban networks in the future.

Under the circumstance of greatly developing renewable energy usage and energy conservation and emission reduction, VSC-HVDC will be applied widely. For example,

ISSN: 2005-4297 IJCA

VSC-HVDC can be used for grid-connected wind farm, which may alleviate voltage fluctuation problem results from output power difference of wind power plant, thus enhancing quality of electric energy; with VSC-HVDC to connect the power to some islets may limit short circuit capacity of interacted system, in the meantime, there is no need to add compensation equipment to DC transmission line in terms of investment, operating cost and long-distance transmission, it has an advantage over AC transmission line; for some power supply system in big cities, not only does VSC-HVDC can resolve voltage flicker and improve power quality of power supply, but it may achieve system damping and enhance system stability; meanwhile, due to VSC-HVDC uses buried DC cable, which is free of alternating magnetic field, no oil pollution and no power transmission corridors required, it may fulfill reformation of capacity expansion of urban power grid without electromagnetic interference or making an impact on city appearance, as well as satisfy requirements of city center load and environmental protection and energy saving.

## 2. Mathematical Model of VSC-HVDC System

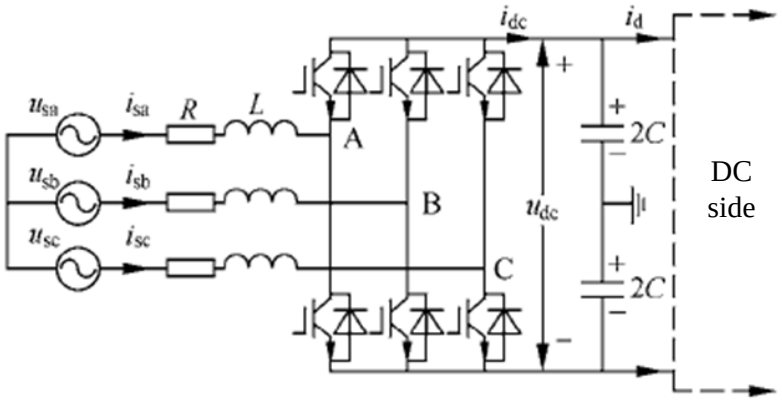


**Figure 1. The Structure of Voltage Source Converter**

Assume that voltage of three-phase network is balanced; the mathematical model under synchronous rotating reference frame is obtained according to topological structure in Figure 1

$$\begin{aligned} L\frac{di_{sd}}{dt} - wLi_{sq} + Ri_{sd} &= u_{sd} - u_d \\ L\frac{di_{sq}}{dt} - wLi_{sd} + Ri_{sd} &= u_{sq} - u_q \\ C\frac{du_{dc}}{dt} &= \frac{3}{2}(s_d i_{sd} + s_q i_{sq}) - i_d \end{aligned} \tag{1}$$

Where: $u_{sd}$ and $u_{sq}$ are d and q axle component of network voltage, respectively; $u_d$ and $u_q$ are d and q axle component of fundamental wave of AC side voltage, respectively; $i_{sd}$ and $i_{sq}$ are d and q axle component of power grid, respectively.

Active power $p_s$ and reactive power $q_s$ under $d-q$ synchronous rotating reference frame can be denoted as:

$$\begin{cases} p_s = \frac{3}{2}\left(u_{sd}i_d + u_{sq}i_q\right) \\ q_s = \frac{3}{2}\left(u_{sd}i_q - u_{sq}i_d\right) \end{cases} \tag{2}$$

 

When $d$ axle is orienting as network voltage vector, namely $u_{sq}=0$, then formula (1-4) can be written as:

$$\begin{cases} p_s = \frac{3}{2} u_{sd} i_d \\ q_s = \frac{3}{2} u_{sd} i_q \end{cases} \tag{3}$$

It can be seen from formula (1-5) that the active and reactive power of converting current of convertor station and alternating current system can be adjusted controlling $i_d$ and $i_q$ respectively.

## 3. Design of ADRC Based System Controller of VSC-HVDC

PI control in VSC-HVDC system is a method of reaching steady state for such system by adjusting controller parameters, but issues like low stability precision and weak anti-jamming capability do exist in such system, it's required to continuously adjust controller parameter according to different operational states. Control structure as shown in Figure 2 and 3 [7, 8]. Auto-disturbance rejection control technology is proposed aiming at above-mentioned problems, the controller of it is comprised of transition process arranging (TD) , extended state observer (ESO) and nonlinear state error feedback (NLSFF).

First of all, TD may rapidly track system's input signal without overshoot, and provide a favorable signal differential to it; second, the total disturbance of whole system in auto-disturbance rejection controller is comprised of uncertain internal disturbance of its own model and external disturbance of system, it directly detects an integrative action of internal and external disturbance but not distinguish them concretely, an evaluation will be made respectively on state and disturbance (internal and external disturbance of system) of system through ESO; at the end, compensation action of disturbance component is obtained using control of NLSFF [11].

Due to ADRC, which requires less calculated amount and has fine robustness of controller, may be applied to decoupling control of multivariable system, it's applied in outer control of convertor station controller in VSC-HVDC, inner loop still uses PI link [12].

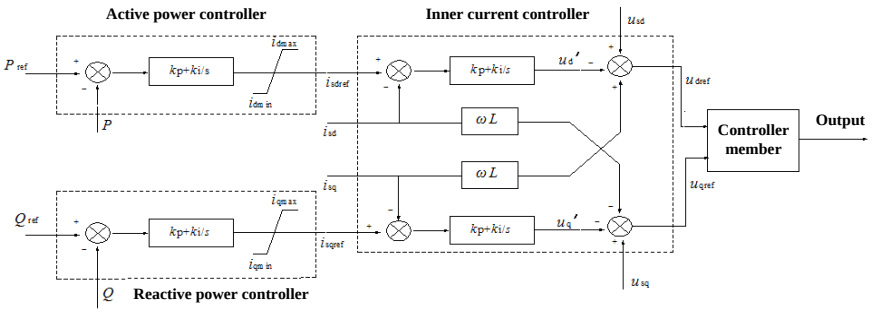


**Figure 2. The Structure Diagram of the Sending System**

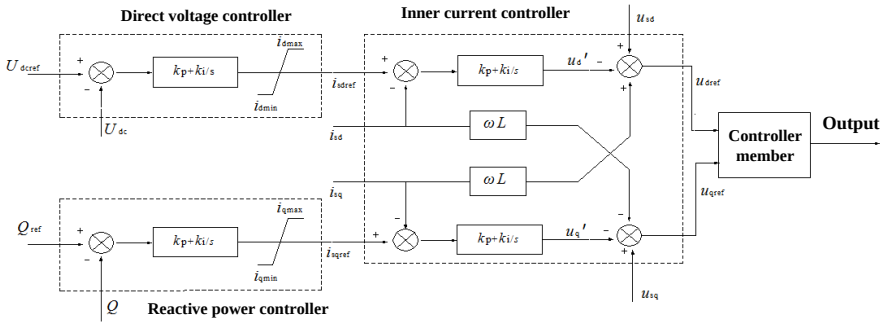


**Figure 3. The Structure Diagram of the Reception System**

### 3.1. Controller Design of Sending System

The sending system adopts strategy of active power controller. Inner current controller adopts PI controller to complete the decoupling control, the design of external loop includes active power controller and reactive power controller.

When the system is running normally, control system requires DC side voltage to keep a steady state and AC side system to run under unit power factor, namely zero reactive power output. Reactive power is only related to $i_{sq}$, therefore, the control object makes $i_{sq}$ track its reference value $i_{sqref}$ with quick localization free of non-overshoot.

#### 3.1.1. Design of Active Power Controller

Obtained from formula (4)

$$P_S = \frac{3}{2} u_{sd} i_{sd} \tag{4}$$

To achieve measured active power to track reference value quickly and accurately and reach a target of simplistic control algorithm and high-speed computation. The controlling unit of active power adopts TD to arrange transient process and employs optimal control function fal to obtain an allowance of electric current $i_{sd}$, and it's used as reference value $i_{sdref}$ of active power inner current after adding with predictive estimation obtained in formula (2-1) [13]. The structure diagram of the active controller as shown in Figure 4.

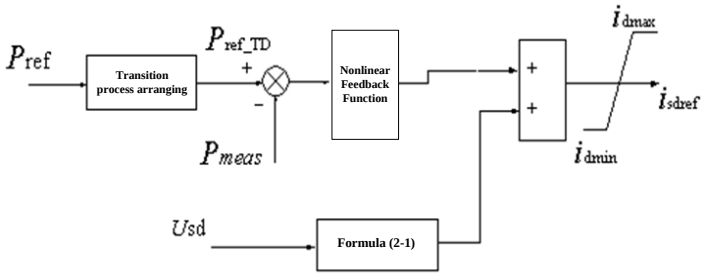


**Figure 4. The Structure of the Active Controller**

It can be seen from the diagram that the controller is comprised of TD , NLSEF and formula (2-1)modules.

① The design of TD

 

To achieve an reasonable transient process and reduce the overshoot of output, transition process arranging TD designed is implemented with classic inertial element,

$$P_{ref\_TD} = \frac{k}{Ts+1} P_{ref} \tag{5}$$

K and T are adjustable parameter, k=1, T=0.05, $P_{ref\_TD}$ in formula is the transition process of preference value $P_{ref}$ of active power, the output $P_{ref\_TD}$ of it is to be an input for NLSEF. The implementation of its matlab as shown in Figure 5.

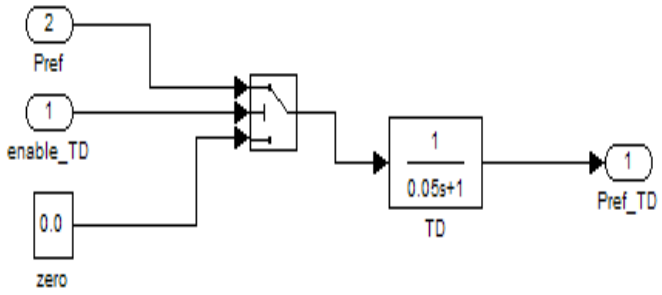


**Figure 5. The Arrangements for Transition**

② The design of NLSEF

NLSEF is constructed according to the error between transition process $P_{ref\_TD}$ and actual value $P_{meas}$ of active power [9]:

$$i_{sdref} = k_1 fal(P_{ref\_TD} - P_{meas}, \alpha_1, \delta_1) \ldots\ldots (2-3)\ k_1 = 1; \alpha_1 = 0.25; \delta_1 = 0.01 \tag{6}$$

The implementation of its Matlab/Simulink as shown in Figure 6.

### 3.1.2. The Design of Reactive Power Controller

Formula of active power obtained from formula (1-4)

$$q_s = \frac{3}{2} u_{sd} i_{sq} \tag{7}$$

When the system is running normally, $u_{sd}$ is nearly constant, in consideration of the effect of static error of system, an allowance of electric current is obtained using optimal control function fal, and it's used as reference value $i_{sdref}$ of current component of q axle after adding with predictive estimation obtained in formula (2-2) [14]. The structure diagram of reactive power controller as shown in Figure 7.

$$i_{sqref} = k_2 fal\ (Q_{ref} - Q_{meas}, \alpha_2, \delta_2) + \frac{2Q_{ref}}{3u_{sd}} \mathrm{K} \tag{8}$$

In formula, $k_2 = 1.8; \alpha_2 = 0.7; \delta_2 = 0.01$

The implementation of its Matlab/Simulink as shown in Figure 8.

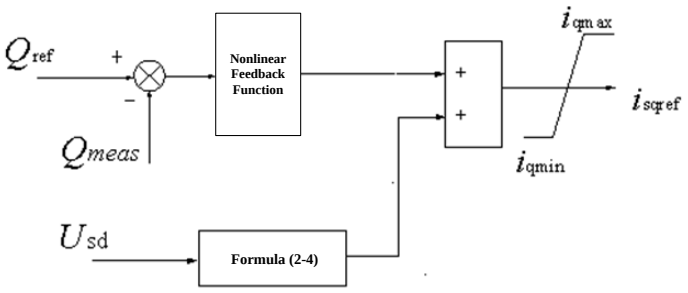


**Figure 6. The Structure of the Reactive Power Controller**

### 3.2. Design of Receiving System Controller

Due to the size DC transmission power is decided by the burdened size of receiving system , because constant DC voltage control is adopted on receiving system in this article, the controller is comprised of inner current controller, external DCV controller and external reactive power controller. Of which inner current controller and reactive power controller are identical in receiving system, so I won't go into detail here.

#### 3.2.1. Design of Constant DC Voltage Controller

VSC-HVDC system is a typical nonlinear, multivariable and strong coupling system, which contains product of state variable and control variable [15]. AC side power in convertor station and DC side power in bridge circuit are equal if the wastage in convertor station is omitted.

Namely:

$$\frac{3}{2}(u_{sd}-Ri_{sd})i_{sd}+\frac{3}{2}(u_{sq}-Ri_{sq})i_{sq}=u_{dc}i_{dc}+u_{dc}C\frac{du_{dc}}{dt} \quad (9)$$

For AC power of three-phase symmetry, $u_{sq}=0$ when orienting as d axle. The effect of $i_q$ shall be omitted in order to obtain unit power in convertor station,

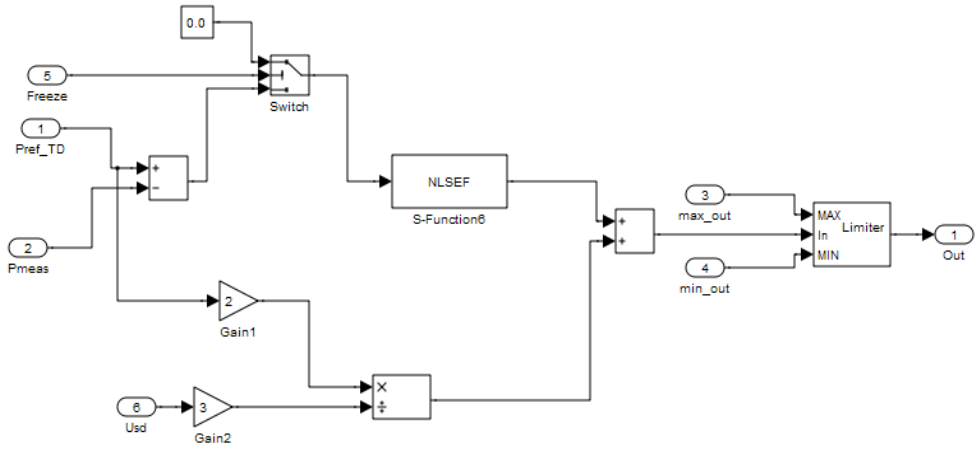


**Figure 7. The Control Structure of NLSEF and ESO**

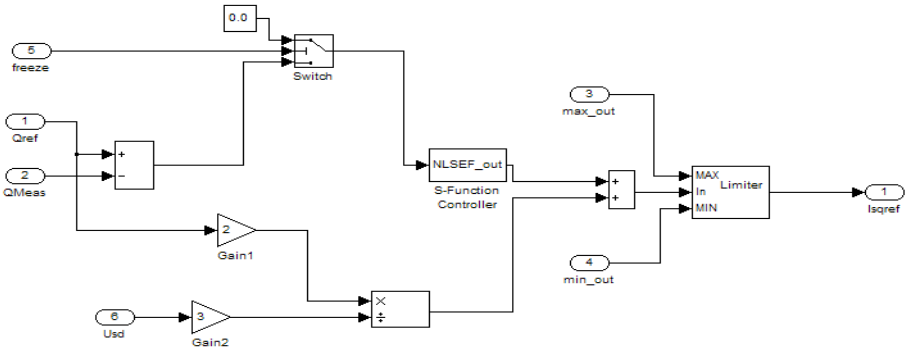


**Figure 8. The Structure of Outer Reactive Power**

then the formula can be written as:

$$\frac{du_{dc}}{dt} = -\frac{i_{dc}}{C} + \frac{3(u_{sd} - Ri_{sd})}{2Cu_{dc}} i_{dc} = f_1 + b_1 u \tag{10}$$

In formula

$$f_1 = -\frac{i_{dc}}{C}, \quad b_1 = \frac{3(u_{sd} - Ri_{sd})}{2Cu_{dc}}, \quad u = i_{dc} \tag{11}$$

The load disturbance $f_1$ can be obtained measuring load current directly, thus leaving out ESO, then the estimated value $z_2$ of disturbance in ADRC is replaced by disturbance $f_1$ in actual measurement. The structure of DC voltage controller as shown in Figure 9.

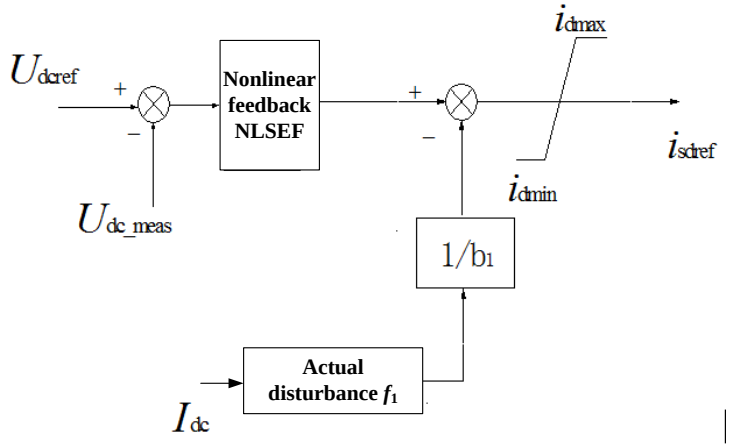


**Figure 9. The Structure of DC Voltage Controller**

Then the current component of d axle is

$$i_{sdref} = k_3 fal(u_{dcref} - u_{dc}, \alpha_3, \delta_3) - \frac{f_1}{b_1} = \tag{12}$$

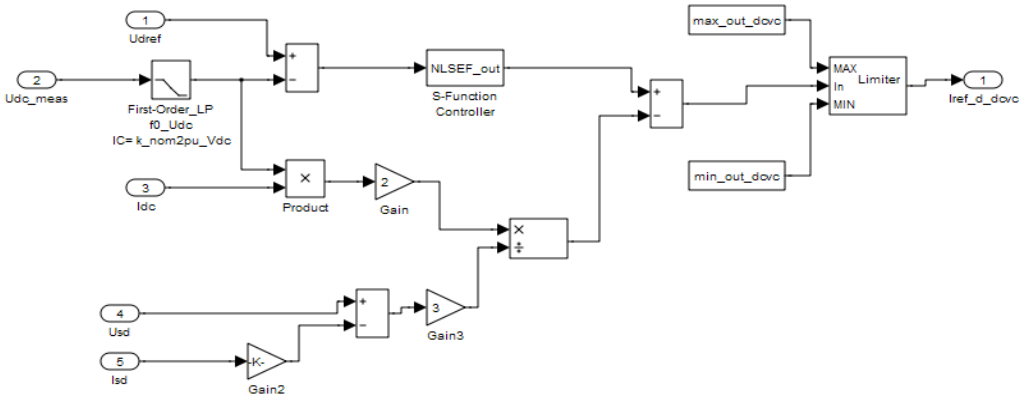


**Figure 10. The Structure of Outer DC Voltage**

$$k_3 fal(u_{dcref} - u_{dc}, \alpha_3, \delta_3) + \frac{2i_{dc}u_{dc}}{3(u_{sd} - Ri_{dc})} \quad (13)$$

where, $k_3$, $\alpha_3$ and $\delta_3$ are adjustable parameter, general value range is an interval length, which in general is a lesser positive number, of linear region, varied size has a slightly effect on control performance, a higher value is normally selected for $k_3$ [16]. The implementation of its Matlab/Simulink as shown in Figure 10.

## 4. Modeling and Simulation of System

Simulation model is established in Matlab/Simulink. In the simulation model, electric power is transported from electric system (AC System1) of 230KV, 2000MVA and 50Hz to electric system (SPWM) of 230KV, 2000MVA and 50Hz through HVDC power transmission line. Rectifier and inverter are built using bridge model of IGBT/anti-parallel diode with multi-level inverters. A 27 times of baseband (1350Hz) single-phase triangular carrier is adopted on the switch of sinusoidal pulse width modulation (SPWM).

### 4.1. Simulation Scenario and Result Analysis

#### 4.1.1. System Response in Inverter When AC Voltage Changed in Inverter Side

When t=0.7s, three-phase AV voltage of sending system turns into 0.9pu from 1pu with time of duration of 0.14s, the simulating curve of it as shown in Figure 11 and 12, simulation time t=1s.

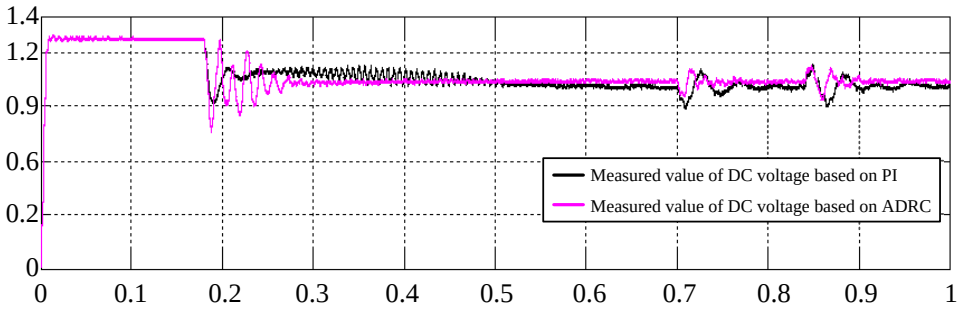


(a) DC voltage of sending end $U_{dc—meas}$ (pu)

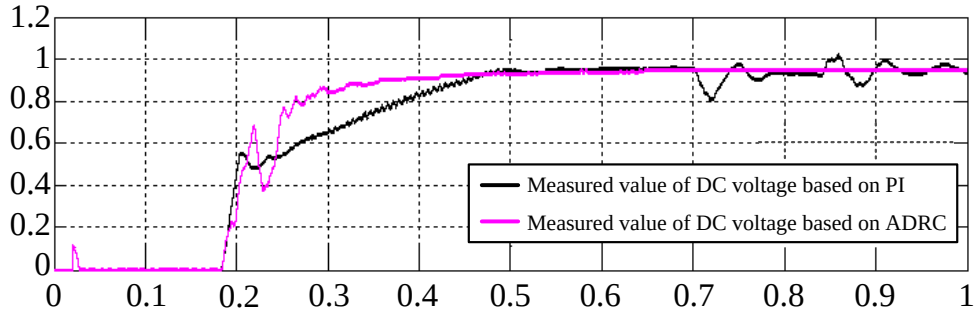


(b) DC voltage of sending end $I_{dc\_meas}$ (pu)

**Figure 11. Simulation Results in Inverter When AC Voltage Changed In Inverter Side**

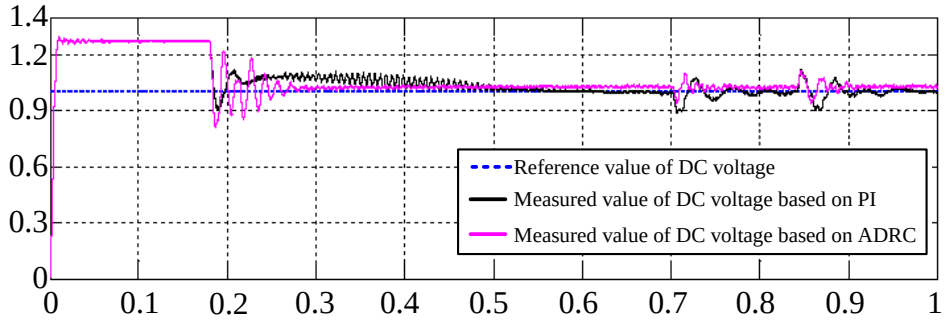


(c) DC voltage of receiving end $U_{dc\_meas}$ $U_{ref}$ (pu)

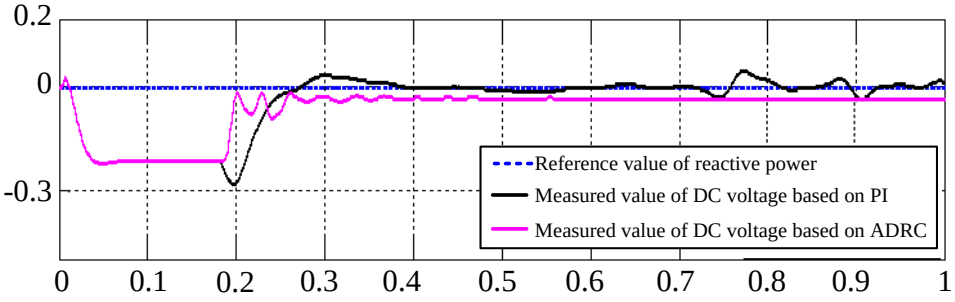


(d) Reactive power of receiving end $Q_{\_meas}$ (pu)

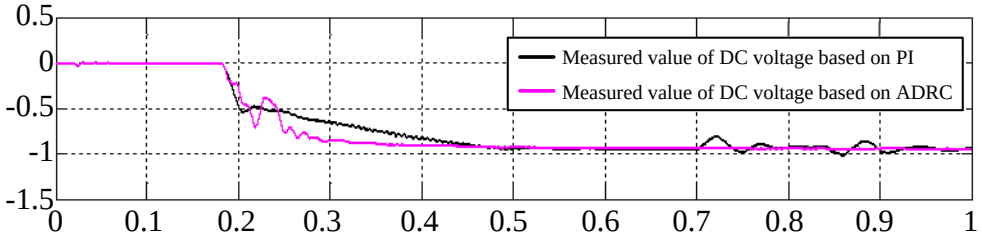


(e) DC of receiving end $I_{dc\_meas}$ (pu)

**Figure 12. Simulation Results in Rectifier When AC Voltage Changed in Inverter Side**

It can be seen from Figure 11 and 12 that the change in alternating voltage of sending system triggers tiny variations of DC voltage, DC current, power in DC side, active power of system in sending system and receiving system, the variation

of reactive power in sending end is significant and there appears to be slight variation of reactive power in receiving end, but ADRC control based DC side voltage and DC side current of controller is lesser than PI control based (Figure 11 (a) (b) and Figure 12 (a) (c)); The variation of reactive power in receiving system based on ADRC control is lesser than PI control based (Figure 12 (b)).

#### 4.1.2. System Response in Inverter when AC Voltage Changed in Inverter Side

Single-phase earth fault occurred in AC side of receiving system when t=0.7s, the time of duration is 0.12s and simulation time t=1.2s, the response curve of system as shown in Figure 13 and 14.

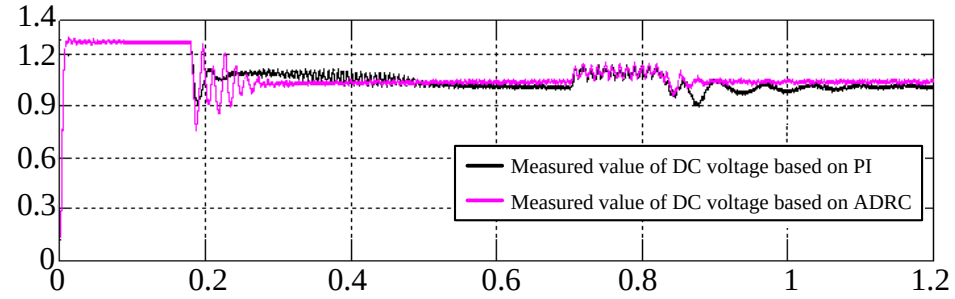


(a) DC voltage in sending end $U_{dc\_meas}$ (pu)

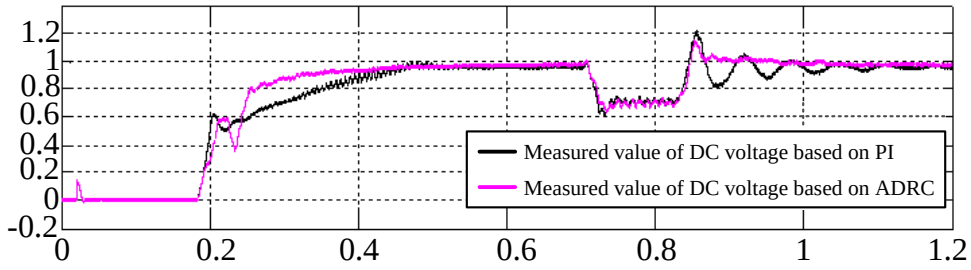


(b) The power of DC side in sending end $P_{dc\_meas}$ (pu)

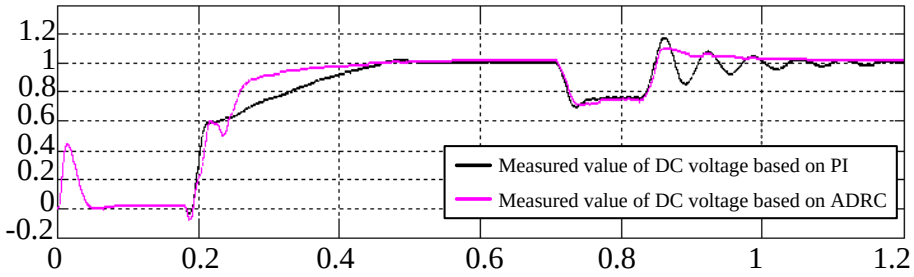


(c) Active power in sending end $P_{\_meas}$ (pu)

**Figure 13. Simulation Results in Inverter When Single-Phase Grounding in Rectifier Side**

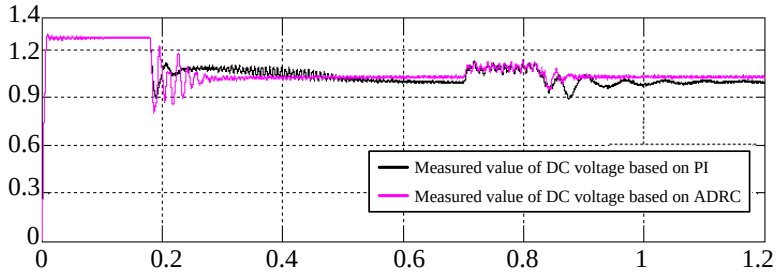


(a) DC voltage in receiving end $U_{dc—meas}$ $U_{ref}$ (pu)

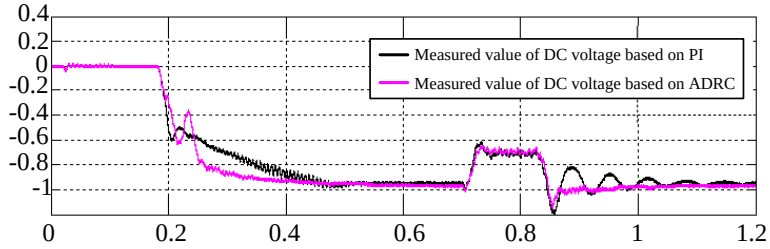


(b) The power of DC side in receiving end $P_{dc—meas}$ (pu)

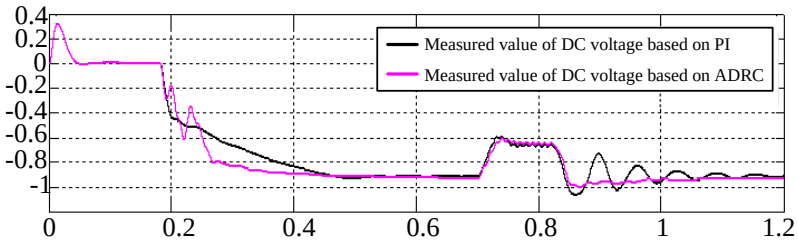


(c) Active power in receiving end $P_{—meas}$ (pu)

**Figure 14. Simulation Results In Rectifier When Single-Phase Grounding in Rectifier Side**

It can be seen from the Figure that there appears to be a vibration (Figure 13 (a) (b) and Figure 14 (a) (b)) of DC voltage and DC side power in sending and receiving system when t=0.7s, and overcurrent phenomena is occurred in sending system side, among of it, three-phase current value of controller based on ADRC control is smaller than PI control based controller (Figure 13 (b) (c)). Fault eliminated when t=0.82s, these two controllers begin to adjust, ADRC based system recovered after approximately 0.1s, however, PI based system still shows up a brief oscillation after the fault being eliminated, it returns to its normal state (Figure 13 (a) (b) (c) and Figure 14 (a) (b) (c)) after approximately 0.3s.

## 5. Conclusion

In conclusion, ADRC based controller designed in this article uses nonlinear function, it has simple control method and higher stability precision and easy to be implemented, such controller is not sensitive to parameters of system controlled and it has strong anti-jamming capability, such controller will make quick response when DC side voltage and reactive power changed and a fault has occurred, in addition, it may adjust the parameters in system to expected target in the shortest time in order to meet the control requirements. When a system failure, PI based controller has slower rapidity, inferior stability and weak anti-jamming capability compared with ADRC based one when a system boots. In general, ADRC based controller is more applicable to VSC-HVDC system.

## Acknowledgement

Project of National Natural Science Foundation of China (11375058) and natural science foundation of Hunan province (13JJ6078)

## References

[1] G. Yan, Y. Lv, Q. Wang and Y. Geng, "Routing algorithm based on delay rate in wireless cognitive radio network", Journal of Networks, vol. 9, no. 4, **(2014)**, pp. 948-955
[2] Y. Lin, J. Yang and Z. Lv, "A Self-Assessment Stereo Capture Model Applicable to the Internet of Things", Sensors, vol. 15, no. 8, **(2015)**, pp. 20925-20944.
[3] K. Wang, X. Zhou and T. Li, "Optimizing load balancing and data-locality with data-aware scheduling", Big Data (Big Data), 2014 IEEE International Conference on. IEEE, **(2014)**: 119-128.
[4] L. Zhang, B. He and J. Sun, "Double Image Multi-Encryption Algorithm Based on Fractional Chaotic Time Series", Journal of Computational and Theoretical Nanoscience, vol. 12, **(2015)**, pp. 1-7.
[5] T. Su, Z. Lv and S. Gao, "3d seabed: 3d modeling and visualization platform for the seabed[C]. Multimedia and Expo Workshops (ICMEW)", 2014 IEEE International Conference on. IEEE, **(2014)**, pp. 1-6.
[6] Y. Geng, J. Chen, R. Fu, G. Bao and K. Pahlavan, "Enlighten wearable physiological monitoring systems: On-body rf characteristics based human motion classification using a support vector machine", IEEE transactions on mobile computing, vol. 1, no.1, **(2015)**, pp. 1-15
[7] Z. Lv, A. Halawani and S. Feng, "Multimodal hand and foot gesture interaction for handheld devices", ACM Transactions on Multimedia Computing, Communications, and Applications TOMM, vol. 11, no. 1s, **(2014)**, pp. 10.
[8] G. Liu, Y. Geng and K. Pahlavan, "Effects of calibration RFID tags on performance of inertial navigation in indoor environment", 2015 International Conference on Computing, Networking and Communications (ICNC), **(2015)**.
[9] J. He, Y. Geng, Y. Wan, S. Li and K. Pahlavan, "A cyber physical test-bed for virtualization of RF access environment for body sensor network", IEEE Sensor Journal, vol. 13, no. 10, **(2013)**, pp. 3826-3836
[10] W. Huang and Y. Geng, "Identification Method of Attack Path Based on Immune Intrusion Detection", Journal of Networks, vol. 9, no. 4, **(2014)**, pp. 964-971
[11] X. Li, Z. Lv and J. Hu, "XEarth: A 3D GIS Platform for managing massive city information", Computational Intelligence and Virtual Environments for Measurement Systems and Applications (CIVEMSA), 2015 IEEE International Conference on. IEEE, **(2015)**, pp. 1-6.
[12] J. He, Y. Geng, F. Liu and C. Xu, "CC-KF: Enhanced TOA Performance in Multipath and NLOS Indoor Extreme Environment", IEEE Sensor Journal, vol. 14, no. 11, **(2014)**, pp. 3766-3774
[13] N. Lu, C. Lu, Z. Yang and Y. Geng, "Modeling Framework for Mining Lifecycle Management, Journal of Networks", vol. 9, no. 3,**(2014)**, pp. 719-725
[14] Y. Geng and K. Pahlavan, "On the accuracy of rf and image processing based hybrid localization for wireless capsule endoscopy", IEEE Wireless Communications and Networking Conference (WCNC), pp. **2015)**
[15] X. Li, Z. Lv and J. Hu, "Traffic management and forecasting system based on 3d gis", Cluster, Cloud and Grid Computing (CCGrid), 2015 15th IEEE/ACM International Symposium on, **(2015)**, pp. 991-998.
[16] S. Zhang and H. Jing, "Fast log-Gabor-based nonlocal means image denoising methods", Image Processing (ICIP), 2014 IEEE International Conference on. IEEE, **(2014)**, pp. 2724-2728.
[17] J. Hu and Z. Gao, "Distinction immune genes of hepatitis-induced heptatocellular carcinoma", Bioinformatics, vol. 28, no. 24, **(2012)**, pp. 3191-3194.

## Authors

**Hu Xiangjuan**, she received her M.S. degree in Circuits and systems from Hunan university in Changsha,China. She is currently a lecturer in the Department of Information Engineering at Shaoyang university. Her research interest is mainly in the area of HVDC, Embedded technology. She has published several research papers in scholarly journals in the above research areas.

 